



# CHORUS

This is the accepted manuscript made available via CHORUS. The article has been published as:

## Charge density wave behavior and order-disorder in the antiferromagnetic metallic series $\text{Eu}(\text{Ga}_{1-x}\text{Al}_x)_4$

Macy Stavinoha, Joya A. Cooley, Stefan G. Minasian, Tyrel M. McQueen, Susan M. Kauzlarich, C.-L. Huang, and E. Morosan

Phys. Rev. B **97**, 195146 — Published 23 May 2018

DOI: [10.1103/PhysRevB.97.195146](https://doi.org/10.1103/PhysRevB.97.195146)

# Charge density wave behavior and order-disorder in the antiferromagnetic metallic series $\text{Eu}(\text{Ga}_{1-x}\text{Al}_x)_4$

Macy Stavinoha<sup>1</sup>, Joya A. Cooley<sup>2</sup>, Stefan G. Minasian<sup>3</sup>, Tyrel M. McQueen<sup>4,5,6</sup>, Susan M. Kauzlarich<sup>2</sup>, C.-L. Huang<sup>7</sup>, and E. Morosan<sup>1,7</sup>

<sup>1</sup>*Department of Chemistry, Rice University, Houston, TX 77005 USA*

<sup>2</sup>*Department of Chemistry, University of California, Davis, CA 95616 USA*

<sup>3</sup>*Chemical Sciences Division, Lawrence Berkeley National Laboratory, Berkeley, CA 94720 USA*

<sup>4</sup>*Institute for Quantum Matter and Department of Physics and Astronomy, The Johns Hopkins University, Baltimore, Maryland 21218 USA*

<sup>5</sup>*Department of Chemistry, The Johns Hopkins University, Baltimore, Maryland 21218 USA*

<sup>6</sup>*Department of Materials Science and Engineering,*

*The Johns Hopkins University, Baltimore, Maryland 21218 USA*

<sup>7</sup>*Department of Physics and Astronomy, Rice University, Houston, TX 77005 USA*

(Dated: April 26, 2018)

The solid solution  $\text{Eu}(\text{Ga}_{1-x}\text{Al}_x)_4$  was grown in single crystal form to reveal a rich variety of crystallographic, magnetic, and electronic properties that differ from the isostructural end compounds  $\text{EuGa}_4$  and  $\text{EuAl}_4$ , despite the similar covalent radii and electronic configurations of Ga and Al. Here we report the onset of magnetic spin reorientation and metamagnetic transitions for  $x = 0 - 1$  evidenced by magnetization and temperature-dependent specific heat measurements.  $T_N$  changes non-monotonously with  $x$ , and it reaches a maximum around 20 K for  $x = 0.50$ , where the  $a$  lattice parameter also shows an extreme (minimum) value. Anomalies in the temperature-dependent resistivity consistent with charge density wave behavior exist for  $x = 0.50$  and 1 only. Density functional theory calculations show increased polarization between the Ga–Al covalent bonds in the  $x = 0.50$  structure compared to the end compounds, such that crystallographic order and chemical pressure are proposed as the causes of the charge density wave behavior.

## I. INTRODUCTION

The interplay of structural, magnetic, and electronic properties of rare earth based intermetallics often results in emergent phenomena and competing ground states, such as unconventional superconductivity, heavy fermion behavior, intermediate valence, and quantum criticality.<sup>1</sup> Particularly, pressure, magnetic field, or chemical doping in Ce and Yb compounds in their magnetic or nonmagnetic sublattices has been extensively used to tune the balance between their versatile ground states.<sup>2-4</sup> Comparatively less work has been done to explore the effects of pressure or doping in Eu-based intermetallics, even though Eu presents similar opportunities to tune the ground state through valence fluctuations between magnetic  $\text{Eu}^{2+}$  and nonmagnetic  $\text{Eu}^{3+}$  ions.<sup>5</sup> In this study, we explored the effects of isovalent doping in the  $\text{Eu}(\text{Ga}_{1-x}\text{Al}_x)_4$  series, motivated by the wide range of apparently conflicting results observed when tuning the properties of the end compounds  $\text{EuGa}_4$  and  $\text{EuAl}_4$ .

Previous studies on single crystals of the stoichiometric compounds  $\text{EuGa}_4$  and  $\text{EuAl}_4$  revealed that the two show similar magnetic behavior, with antiferromagnetic (AFM) ordering and very similar Néel temperatures  $T_N = 15$  K and 15.4 K, respectively.<sup>6-8</sup> The compounds are isostructural, forming in a tetragonal crystal structure consisting of two distinct transition metal sites, forming a covalently-bound anionic framework with divalent body-centered cations. The structural and magnetic similarities between these two compounds may be easily understood considering the chemical similarities of Ga and

Al: they are isovalent, with very close covalent radii of 1.22 Å and 1.21 Å, respectively.<sup>9</sup> However, drastic differences have also been noted with either doping or applied pressure, which cannot be readily explained. While no evidence for mass renormalization has been reported in  $\text{EuAl}_4$ , electrical resistivity measurements have suggested heavy fermion behavior in  $\text{EuGa}_4$ .<sup>7,8</sup> At ambient pressure, a plausible charge density wave (CDW) was reported for  $\text{EuAl}_4$  below  $T^* = 140$  K, and increasing pressure suppressed  $T^*$  to zero for  $p = 2.5$  GPa. However, in  $\text{EuGa}_4$ , a plausible CDW is observed *only* under applied pressure, with  $T^* = 105$  K for  $p = 0.75$  GPa, which subsequently increased to 160 K for  $p = 2.15$  GPa. Doping  $\text{EuM}_4$  ( $M = \text{Ga}$  or  $\text{Al}$ ) on either the magnetic (Eu) or nonmagnetic ( $M$ ) sublattice has also shown notable changes in the magnetic, electronic, and crystallographic properties. When Eu is substituted by Yb in  $(\text{Eu}_{0.5}\text{Yb}_{0.5})\text{Ga}_4$ ,  $T_N$  is suppressed to 13 K.<sup>10</sup> On the other hand, doping  $\text{EuGa}_4$  in the nonmagnetic sublattice has shown that the AFM order is suppressed to  $T_N = 9.6$  K and 6.3 K in polycrystalline  $\text{Eu}(\text{Ga}_{1-x}\text{Al}_x)_4$  ( $A, x$ ) = (Mg,0.14) or (Li,0.18), respectively.<sup>11</sup> In contrast,  $\text{EuAl}_4$  doped with Si resulted in ferromagnetic (FM) order below  $T_C = 17$  K in  $\text{Eu}(\text{Al}_{0.75}\text{Si}_{0.25})_4$ .<sup>12</sup>

The versatile interplay between spin and charge degrees of freedom in  $\text{EuM}_4$  motivates the current systematic study of the solid solution between the Ga and Al end compounds in the series  $\text{Eu}(\text{Ga}_{1-x}\text{Al}_x)_4$  with  $x = 0$  to 1. Such a substitution should minimize the chemical effects brought about by doping, since replacing Ga with isoelectronic and similarly-sized Al does not change the

electron count or the volume of the unit cell (and hence the chemical pressure). Thermodynamic and transport measurements on  $\text{Eu}(\text{Ga}_{1-x}\text{Al}_x)_4$  single crystals reveal strong correlations between the structural, magnetic, and electronic properties. The compounds remain tetragonal with space group  $I4/mmm$  at room temperature for the whole doping range, with Ga and Al preferentially occupying one or the other of the two transition metal element sites. Remarkably, for  $x = 0.50$ , the two transition metals fully separate into two sublattices and form an ordered structure  $\text{EuGa}_2\text{Al}_2$  with a minimum unit cell volume in the series. This, in turn, favors the occurrence of a plausible CDW state at ambient pressure at  $T^* = 51$  K, while  $T_N$  is maximum in this composition at  $\sim 20$  K. These results should be contrasted with those from isoelectronic doping ( $\text{Ca}^{2+}$  or  $\text{Sr}^{2+}$ ) or hole doping ( $\text{La}^{3+}$ )<sup>13</sup> in  $\text{EuGa}_4$  on the magnetic sublattice, where in some cases structural distortions preclude the occurrence of a CDW transition down to 2 K.

## II. EXPERIMENTAL METHODS

Single crystals of  $\text{Eu}(\text{Ga}_{1-x}\text{Al}_x)_4$  were grown by a self-flux technique. Elemental metals were assembled in alumina crucibles with a 1:9 ratio of Eu:Ga/Al. In a typical growth, the metals were melted and homogenized at 900°C and cooled to 700°C at 3°C/hour in an inert argon atmosphere. Single crystals were separated from the flux using centrifugation through an alumina strainer placed between the crucibles. Powder x-ray diffraction was performed at ambient and low temperatures using a Bruker D8 Advance equipped with a Bruker MTC-LOWTEMP sample stage with  $\text{Cu K}\alpha$  radiation. Rietveld refinements were done using the FullProf program suite.<sup>14</sup> Single crystal x-ray diffraction was performed using a Bruker Apex II diffractometer or a Rigaku SCX Mini diffractometer with  $\text{Mo K}\alpha$  radiation. Integration of raw frame data was done using Bruker Apex II software or CrystalClear 2.0. Refinement of the diffraction data was performed using XPREP and ShelXTL software packages.

Electron microprobe analysis (EMPA) was performed using a Cameca SX-100 electron probe microanalyzer with a wavelength-dispersive spectrometer. An accelerating potential of 15 kV and a beam current of 20 nA in a 1  $\mu\text{m}$  fixed beam were used to collect elemental intensities from 15 representative points on a polished surface of each crystal. The composition of each crystal was determined using the averages and standard deviations of the elemental intensities of Eu, Ga, and Al. The elemental intensities of Eu and Ga were determined from a standard sample of  $\text{EuGa}_4$ , and the elemental intensity of Al was similarly determined from a standard sample of  $\text{Al}_2\text{O}_3$ . Chemical formulas for each crystal were calculated assuming 5 atoms per formula unit and full occupancy of the Ga/Al site. The compositions obtained from EMPA and single crystal XRD free variable refinement were used

to determine the doping fractions reported throughout this work with an error of  $\pm 3\%$  in the composition.

Single energy images, elemental maps, and Eu  $M_{5,4}$ -edge x-ray absorption spectra (XAS) were acquired using the scanning transmission x-ray microscope instrument at the spectromicroscopy beamline 10ID-1 at the Canadian Light Source according to data acquisition methodology described previously.<sup>15,16</sup> Samples were prepared by grinding crystals of the analyte into a fine powder with a mortar and pestle and brushing the powder onto carbon support films (3-4 nm carbon, Electron Microscopy Sciences) with a fiber, which arranged a large number of micron-sized particles in a compact area suitable for Eu  $M_{5,4}$ -edge XAS.

DC magnetic susceptibility measurements were performed using a Quantum Design Magnetic Properties Measurement System. Heat capacity measurements were performed by adiabatic thermal relaxation technique using a Quantum Design Physical Properties Measurement System (PPMS). Temperature-dependent ac resistivity measurements were performed using a Quantum Design PPMS with the current  $i = 2$  mA and  $f = 462.02$  Hz for a duration of 7 seconds with  $i \parallel ab$ .

## III. RESULTS

### A. Crystallography

Single crystals of  $\text{Eu}(\text{Ga}_{1-x}\text{Al}_x)_4$  with dimensions of approximately  $3 \times 2 \times 1$  mm<sup>3</sup> were grown for  $x = 0, 0.18, 0.33, 0.50, 0.68,$  and  $1$ . Powder x-ray diffraction at 300 K indicates that all crystals in this series crystallize in the tetragonal  $I4/mmm$  space group. A typical Rietveld analysis is shown for  $x = 0.50$  in Fig. 1, indicating no significant flux inclusions or impurity phases. Temperature-dependent powder x-ray diffraction measurements (Appendix Fig. S1) on  $\text{EuAl}_4$  at  $T = 300$  K and 93 K confirm that the tetragonal crystal structure is preserved down to low temperatures with no structural phase transition, as was reported in some isostructural  $\text{BaAl}_4$ -type structures.<sup>17</sup> Single crystal x-ray refinements confirm the  $I4/mmm$  space group in all compounds reported herein and indicate full occupancy of all lattice sites. In  $\text{EuGa}_4$  and  $\text{EuAl}_4$ , the Ga and Al atoms occupy two inequivalent crystallographic sites corresponding to the  $4d$  site,  $M(1)$ , at  $(0, \frac{1}{2}, \frac{1}{4})$  and the  $4e$  site,  $M(2)$ , at  $(0, 0, z)$ . Upon substituting Ga for Al, a clear site preference is shown: Al fully occupies the  $4d$  site before occupying the  $4e$  site. Diffraction data for single crystal x-ray refinements can be found in the Appendix in Table S1.

### B. Physical Properties

Eu  $M_{5,4}$ -edge x-ray spectromicroscopy was used to probe electronic structure and bonding in selected samples of  $\text{Eu}(\text{Ga}_{1-x}\text{Al}_x)_4$  with  $x = 0, 0.18, 0.50,$  and  $1$ .

In general, each of the Eu  $M_5$ - and  $M_4$ -edges exhibits characteristic multiplet splitting patterns with fine structure that closely resembles expectations from earlier Eu  $M_{5,4}$ -edge studies of divalent Eu compounds.<sup>18,19</sup> Preliminary calculations in the atomic limit for  $\text{Eu}^{2+}$  that described transitions from  $3d^{10}4f^7$  to  $3d^{10}4f^8$  states also reproduced the salient features of the experimental spectra, including the high energy shoulders observed at approximately 1132.5 eV as shown in Appendix Fig S2. Hence, the Eu  $M_{5,4}$ -edge spectra support a ground state  $\text{Eu}^{2+}$  valence formulation for each  $\text{Eu}(\text{Ga}_{1-x}\text{Al}_x)_4$  compound, and no evidence for mixed valence character was detected.

Previous reports showed AFM order in  $\text{EuGa}_4$  and  $\text{EuAl}_4$  at  $T_N = 15$  K and 15.4 K, respectively, and the appearance of spin reorientation transitions in  $\text{EuAl}_4$ .<sup>6,8</sup> However, in the doped series  $\text{Eu}(\text{Ga}_{1-x}\text{Al}_x)_4$  it appears that, as Al replaces Ga(1) at the 4d site, multiple spin reorientation transitions occur, while  $T_N$  changes non-monotonously with  $x$ . Magnetic susceptibility measurements with  $H\parallel ab$  and  $H\parallel c$  are shown in Figs. 2(a) and 2(b). As many as three magnetic transitions occur down to 1.8 K in  $x = 0.50$  and  $x = 1$ . The magnetic transition temperatures were determined from the temperature derivative of magnetization  $d(MT)/dT$  and  $C_p(T)$  data.<sup>20</sup> Even though the end compounds order at virtually identical  $T_N$  values, it appears that the ordering temperature is significantly enhanced at intermediate compositions, and is maximum at  $T_N = 19.0$  K near the ordered

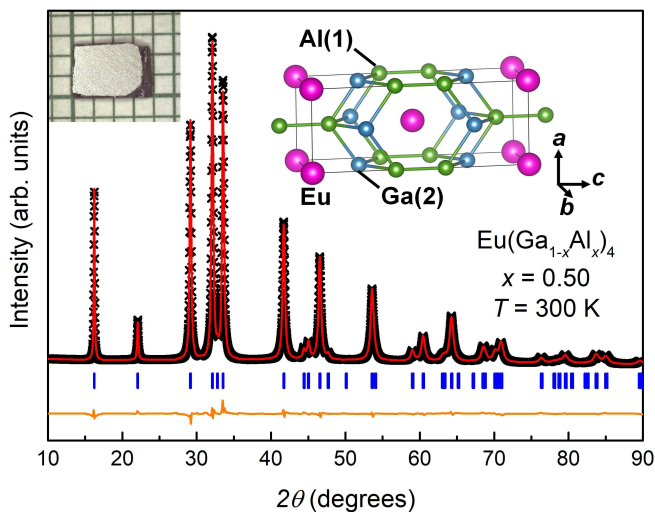


FIG. 1: Powder x-ray diffraction (black symbols) of a doped single crystal of  $\text{Eu}(\text{Ga}_{1-x}\text{Al}_x)_4$  with  $x = 0.50$  indicates that this crystal (and all crystals in this doped series) crystallizes in the  $I4/mmm$  space group with no significant flux inclusion or impurity phases. The red line is the diffraction pattern calculated from Rietveld refinement and the blue ticks are the calculated peak positions. The orange line is the difference between the measured points and the calculated diffraction. The left inset is a picture of a crystal with each square = 1 mm x 1 mm, and the right inset shows the tetragonal crystal structure.

structure at  $x = 0.50$  (purple, Fig. 2). A summary of the magnetic transition temperatures for these compounds is given in Appendix Table S2.

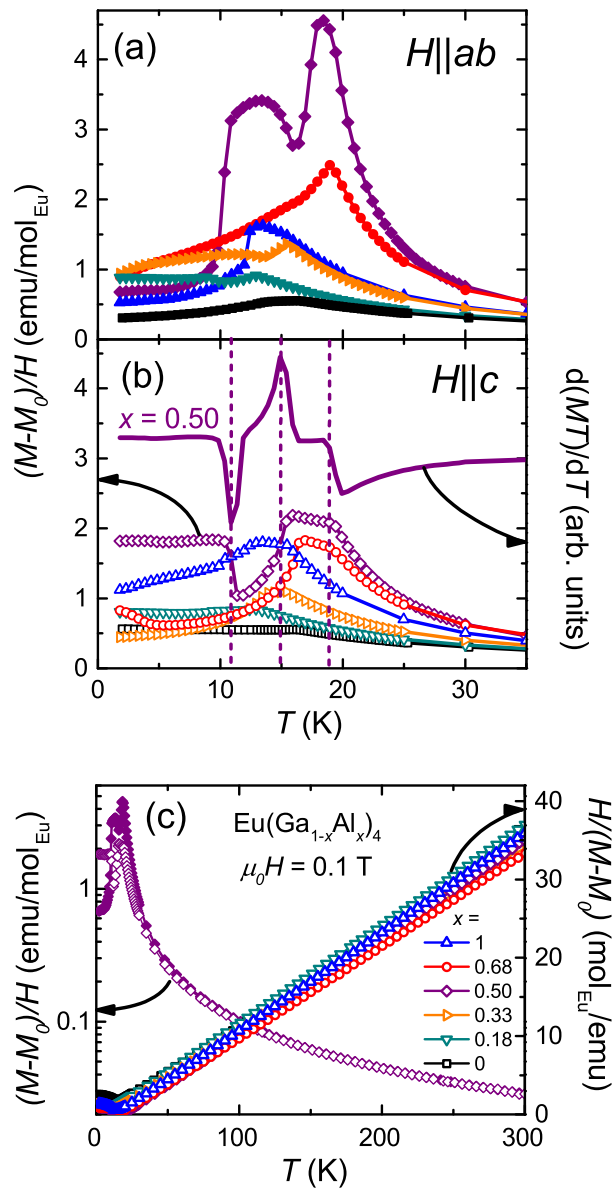


FIG. 2: Temperature-dependent magnetic susceptibility data with (a)  $H\parallel ab$  and (b) left:  $H\parallel c$ . Right: Peaks determined from  $d(MT)/dT$  were used to indicate  $T_N$  and spin reorientation transition temperatures. At high temperatures, (c) left:  $(M - M_0)/H$  for  $x = 0.50$  with closed symbols representing  $H\parallel ab$  and open symbols representing  $H\parallel c$ . Right: the inverse magnetic susceptibility of the polycrystalline average indicates that these crystals show Curie-Weiss behavior and fully divalent Eu ions.

High-temperature inverse magnetic susceptibility  $H/(M - M_0)$  indicates Curie-Weiss behavior across the series as  $H/(M - M_0)$  are linear (Fig. 2(c)) above  $\sim 25$  K. The temperature-independent contribution to the magnetic susceptibility  $M_0$  was subtracted in the case of

EuGa<sub>4</sub>. The linear fits are used to determine the effective magnetic moment  $p_{eff}$  and Weiss temperatures  $\theta_W$ , and these are listed in Appendix Table S2. The  $p_{eff}$  values are comparable to the theoretical  $p_{eff}^{theory} = 7.94$  for Eu<sup>2+</sup>, while the  $\theta_W$  values are positive and close to the  $T_N$  temperatures for the whole series. Positive  $\theta_W$  values are indicative of FM correlations, which were also observed in an isostructural compound EuRh<sub>2</sub>Si<sub>2</sub>.<sup>22</sup>

No crystal electric field (CEF) effects are expected for Eu<sup>2+</sup> ions, and this is indeed consistent with identical  $H||ab$  and  $H||c$  high temperature curves, with the  $x = 0.50$  data shown in Fig. 2(c) as an example. However, in the ordered state, slight differences in  $(M - M_0)/H$  are observed due to the moment orientation relative to the applied field below 50 K, as shown in Figs. 2(a) and 2(b). This is even better evidenced by the anisotropic  $M(H)$  isotherms measured at  $T = 1.8$  K (Figs. 3(a) and 3(b)). The magnetization saturation for all measured compounds, except  $x = 0$ , is  $7 \mu_B/\text{Eu}^{2+}$ , as expected for the  $J = 7/2$  Hund's rule ground state multiplet. EuGa<sub>4</sub> (black squares, Figs. 3(a) and 3(b)) appears to approach saturation slightly above the 7 T maximum field for these measurements. As Al replaces Ga across the Eu(Ga<sub>1-x</sub>Al<sub>x</sub>)<sub>4</sub> series, metamagnetic (MM) transitions are observed for  $x = 0.33, 0.50, 0.68,$  and  $1$  with crystallographic anisotropy. Figure 3(c) shows an example of how the MM critical fields were determined from the peaks in  $dM/dH$ . As expected, the number of MM transitions at low  $T$  (Fig. 3,  $T = 1.8$  K) coincides with the number of transitions in the low  $H$  magnetic susceptibility (Fig. 2).

Specific heat measurements (Fig. 4) confirmed the presence of multiple magnetic transitions in these compounds, with the transition temperatures consistent with those derived from temperature-dependent magnetization measurements. Nakamura et al. argued for heavy fermion behavior in EuGa<sub>4</sub> based on a Fermi liquid relation between the measured quadratic resistivity coefficient  $A$  and the calculated electronic specific heat coefficient  $\gamma$  with a modest mass renormalization from  $\gamma = 138$  mJ/mol K<sup>2</sup>.<sup>8</sup> However, our low temperature  $C_P/T$  data show no evidence for strong mass renormalization in any of the Eu(Ga<sub>1-x</sub>Al<sub>x</sub>)<sub>4</sub> compounds ( $x = 0 - 1$ ), as shown in the inset of Fig. 4.

No Kondo correlations are present in the  $H = 0$  electrical resistivity of Eu(Ga<sub>1-x</sub>Al<sub>x</sub>)<sub>4</sub> (Fig. 5). For all  $x$  values, the high temperature resistivity decreases with  $T$ , until loss of spin disorder scattering at  $T_N$  is marked by an abrupt drop. The residual resistivity ratios RRR =  $\rho(300\text{K})/\rho_0$  (listed in Appendix Table S2) with  $\rho_0 = \rho(2\text{K})$  are an order of magnitude larger for the end compounds ( $x = 0$  and  $1$ ) compared to the doped samples. Remarkably, we observed a sharp resistivity increase occurring for  $x = 0.50$  and  $1$  around 51 and 140 K, respectively. In the latter compound, Nakamura et al.<sup>8</sup> associated the resistivity increase at 140 K with a CDW-like transition. Notably, such a transition appears in Eu(Ga<sub>1-x</sub>Al<sub>x</sub>)<sub>4</sub> *only* for  $x = 0.50$ , where (i)  $x$ -ray

diffraction indicates an ordered structure, with Ga and Al fully occupying the two separate sublattices to form EuGa<sub>2</sub>Al<sub>2</sub>, and (ii) resistivity measurements reveal the lowest residual resistivity  $\rho_0$  and an enhanced RRR value compared to all other doped (disordered) samples.

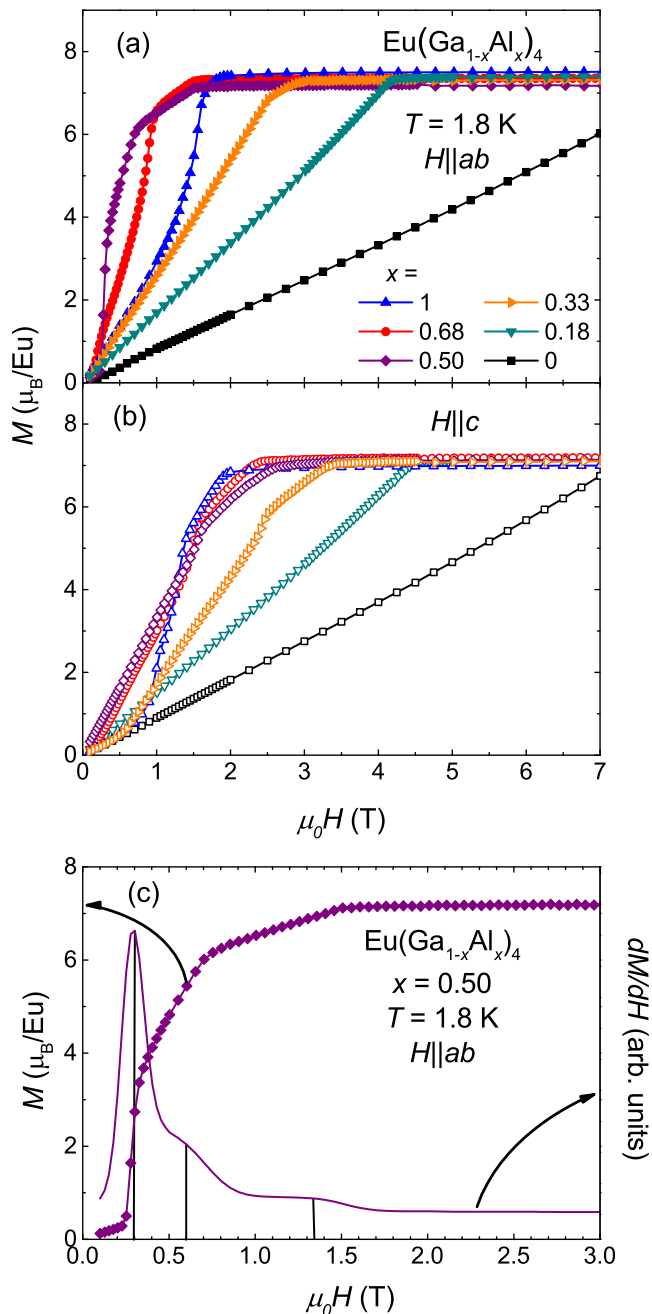


FIG. 3: Field-dependent magnetization curves for (a)  $H||ab$  and (b)  $H||c$  show multiple metamagnetic transitions that are anisotropic. An example of a metamagnetic transition in this series is shown in (c) with an example of how critical fields were determined using peaks from  $dM/dH$  vs.  $H$ .

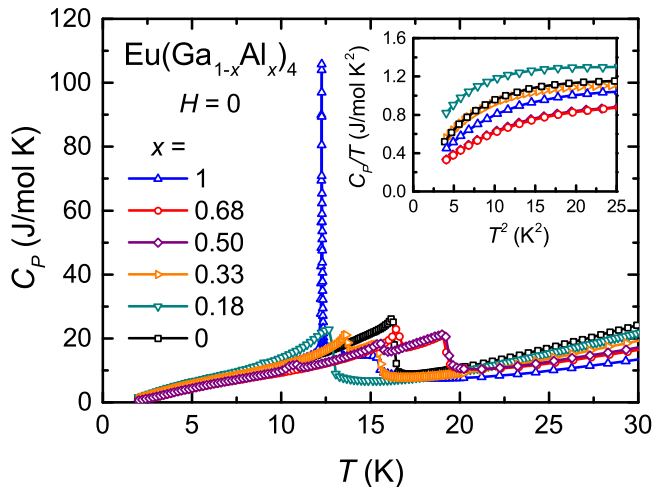


FIG. 4: Specific heat measurements confirm multiple magnetic transitions and a first-order phase transition in  $\text{EuAl}_4$ . The inset shows no evidence of mass renormalization in this system from  $C_P/T$  vs.  $T^2$ .

#### IV. DISCUSSIONS AND CONCLUSIONS

Given the chemical similarities between Ga and Al (isoelectronic, similar covalent radii of 1.22 Å and 1.21 Å, respectively<sup>9</sup>), no substantive differences in crystallographic or physical properties are expected between the isostructural  $\text{EuGa}_4$  and  $\text{EuAl}_4$  compounds. However, as Al replaces Ga in  $\text{Eu}(\text{Ga}_{1-x}\text{Al}_x)_4$ , the magnetic, electronic, and structural properties change non-monotonously: (i) As shown in Fig. 6a, a maximum  $T_N$  occurs in  $x = 0.50$ . This is the result of the minimum Eu–Eu ion spacing in this composition as evi-

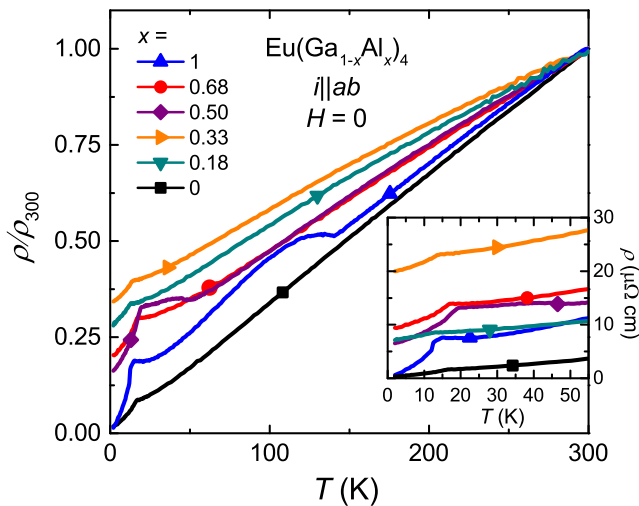


FIG. 5: Temperature-dependent resistivity scaled by  $\rho_{300}$ . Anomalies in  $x = 0.50$  and 1 are consistent with CDW-like behavior. Inset: Absolute resistivity values at low temperatures.

denced by the non-linear change in the  $a$  lattice parameter and unit cell volume (squares and diamonds, respectively, Fig. 6b), which are minimum for  $x = 0.50$ , while  $c$  (triangles) increases linearly from  $x = 0$  to 1. The ground state across the series is AFM (Fig. 2), even though the spin correlations appear FM ( $\theta_W > 0$ ,  $\theta_W \sim T_N$ ). In the absence of frustration or CEF effect, magnetic order is likely a result of strong next-nearest-neighbor interactions (with exchange coupling  $J_2 > 0$ ), in addition to the nearest neighbor Rudermann-Kittel-Kasuya-Yosida coupling (exchange coupling  $J_1 < 0$ ), such that  $J_2 > |J_1|$ <sup>21</sup>. This is consistent with the proposed magnetic structure of  $\text{EuGa}_4$ , where intra-plane Eu magnetic moments are thought to couple ferromagnetically, while inter-plane Eu magnetic moments couple antiferromagnetically.<sup>22</sup> (ii) The observation of a possible CDW transition in  $\text{Eu}(\text{Ga}_{1-x}\text{Al}_x)_4$  with  $x = 0.50$  and 1 may stem directly from the ordered structure, considering the evidence for full site separation for Ga and Al in the  $x = 0.50$  compound. This, however, does not explain the lack of a CDW in the  $x = 0$  (also ordered) analogue, even though applied pressure appeared to induce such a transition.<sup>7</sup> Additional qualitative differences exist even in the pressure-dependence of the plausible CDW transition in  $\text{EuGa}_4$  and  $\text{EuAl}_4$ . According to the change in lattice parameters shown in Fig. 6(b), it seems that Al substituting for Ga acts as positive pressure, resulting in the occurrence of a CDW at  $x = 0.50$  in  $\text{Eu}(\text{Ga}_{1-x}\text{Al}_x)_4$ , similar to the behavior in  $\text{EuGa}_4$  under applied pressure. (iii) Most notable of the non-monotonous trends in this series is the minimum in the in-plane lattice parameter  $a$  at  $x = 0.50$  compared to the linear increase in  $c$  across the entire series (Fig. 6(b)). In order to explain this non-linear structural trend, density functional theory (DFT) calculations with the local density approximation (LDA) were carried out in the linear muffin tin orbital tight binding atomic spheres approximation (LMTO-TB-ASA) to probe the bonding character between Al and Ga in the doped compounds.

DFT calculations were performed for  $x = 0, 0.50$ , and 1. To avoid complications arising from the unpaired  $f$  electrons of  $\text{Eu}^{2+}$ ,  $\text{Sr}^{2+}$  was substituted as an analog in the calculations. In order to ensure that the non-linear changes in  $a$  were associated solely with the Ga–Al bonds and not the Eu atoms, single crystals of  $\text{SrGa}_4$ ,  $\text{SrGa}_2\text{Al}_2$ , and  $\text{SrAl}_4$  were grown from self-flux, and their lattice parameters were measured from powder x-ray diffraction (shown in Appendix Fig. S3). Trends in lattice parameters similar to those in the Eu analogues were observed, with  $a$  minimized in  $\text{SrGa}_2\text{Al}_2$  and  $c$  increasing linearly from  $\text{SrGa}_4$  to  $\text{SrAl}_4$ . As expected from the isoelectronic nature of the series, all three band structures are qualitatively very similar (Appendix Fig. S4). However, analysis of the electron distribution extracted from the integrated density of states (DOS) up to  $E_F$  reveals substantive differences between the end compounds and the  $x = 0.50$  composition: there is charge transfer from the  $M(1)$  to the  $M(2)$  site as the composition approaches

$x = 0.50$  from both end compounds, such that the  $M(1)$  [ $M(2)$ ] electron density is minimum [maximum] for  $x = 0.50$  (see Appendix Table S3). This maximum charge transfer manifests when the two  $M$  sites are preferentially occupied by  $M(1) = \text{Al}$  and  $M(2) = \text{Ga}$ , implying an enhanced polarization of the  $M(1) - M(2)$  covalent bond at  $x = 0.50$  compared to both  $x = 0$  and 1. Despite the similar trends toward less polarization in the Al-rich and Ga-rich compounds, the increased polarization from  $x = 0$  to  $x = 0.50$  prevents bond length expansion (as

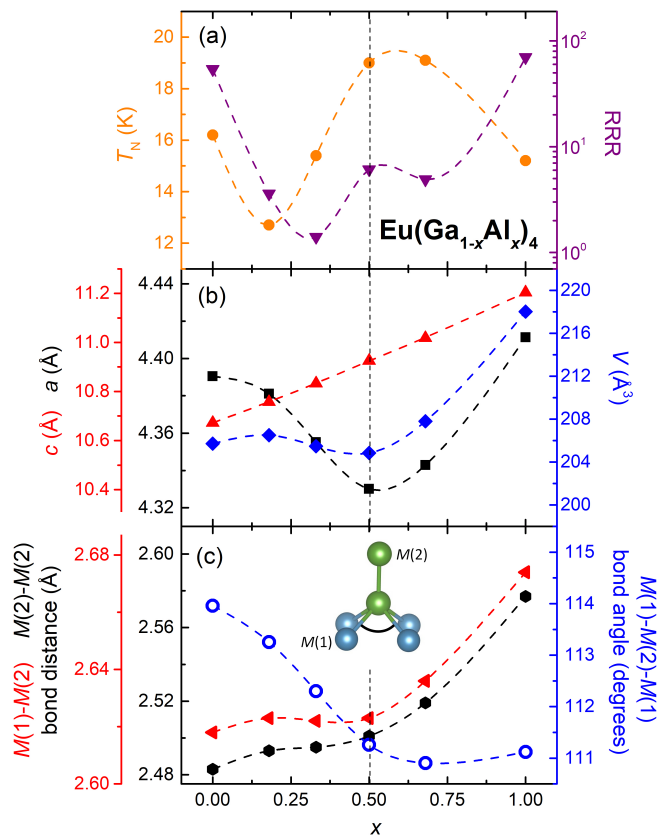


FIG. 6: (a) Left: Increasing  $x$  corresponds to a non-monotonic change in  $T_N$  (orange circles) that could be associated with changes in lattice parameters  $a$  and  $c$ . Right: RRR values (purple down triangles) calculated from resistivity measurements show the low amount of disorder in the end compounds and the decreased disorder in  $x = 0.50$  compared to other doped compounds in the series. (b) Left: Lattice parameters  $a$  (black squares) and  $c$  (red triangles) as a function of doping fraction  $x$  indicating a linear change in  $c$  and a non-linear change in  $a$  with increasing  $x$  resulting in a local minimum. Right: Unit cell volume  $V$  (blue diamonds) as function of  $x$ . (c) Left: Bond distances between atoms located at the  $M(1) - M(2)$  (red left triangles) and  $M(2) - M(2)$  (black hexagons) crystallographic sites remain constant up to  $x = 0.50$  but increase from  $x = 0.50$  to 1. Right: The tetrahedral bond angle between  $M(1) - M(2) - M(1)$  atoms (blue open circles) decreases up to  $x = 0.50$  and remains constant from  $x = 0.50$  to 1. All dashed lines are guides to the eye.

$M(1)$  is replaced by Al but  $M(2)$  remains occupied by Ga), but then polarization is reduced again from  $x = 0.50$  to  $x = 1$  (as  $M(2)$  is also replaced by Al), resulting in a greater increase in bond lengths.

This unexpected deviation from Vegard's law<sup>23</sup> can be further explained by examining the trends in the  $M(1) - M(2)$  and  $M(2) - M(2)$  bond lengths and the  $M(1) - M(2) - M(1)$  bond angle, where  $M = \text{Al}$  or Ga. As shown in Fig. 6(c), as Al occupies the  $M(1)$  site up to  $x = 0.50$ , the bond distance between  $M(1)$  and Ga(2) remains relatively unchanged. However, the bond angle  $M(1) - \text{Ga}(2) - M(1)$  in the Ga-centered tetrahedron decreases linearly up to  $x = 0.50$ . These crystallographic trends acting together expand the  $c$  lattice parameter while simultaneously contracting the  $a$  lattice parameter to a minimum. As Al substitutes Ga in the  $M(2)$  site up to  $x = 1$ , a different trend emerges. Here we observe that the tetrahedral bond angle remains constant while the bond lengths between Al(1) -  $M(2)$  and  $M(2) - M(2)$  increase, thus leading to both lattice parameters  $a$  and  $c$  increasing. These behaviors are likely caused by the greater electronegativity of Ga, which renders the Ga-Ga bonds more polarized.

In summary, we have observed that although Ga and Al are very similar in their valence and size, the substitution of Ga with Al in the doped system  $\text{Eu}(\text{Ga}_{1-x}\text{Al}_x)_4$  produces striking and unexpected magnetic, electronic, and structural transitions. The substitution of Ga with Al up to  $x = 0.50$  decreases  $a$  to a minimum and appears to increase the ferromagnetic interactions in the system, resulting in higher  $T_N$  and multiple magnetic transitions. Additionally, temperature-dependent  $\rho(T)$  measurements show pronounced changes in electronic transport as manifested by CDW formation in  $\text{Eu}(\text{Ga}_{1-x}\text{Al}_x)_4$  for  $x = 0.50$  and 1. The CDW behavior is markedly different between  $\text{EuAl}_4$  and  $\text{EuGa}_4$ , and chemical *and* hydrostatic pressure can be used as tools to elucidate the factors contributing to the CDW formation in this series. Future studies will aim to distinguish between the effects of doping in the magnetic versus the nonmagnetic sublattice in  $\text{EuGa}_4$  and to explore the effects of hole-doping, positive chemical pressure, and disorder on the magnetic and electronic properties of  $\text{EuGa}_4$ .

## V. ACKNOWLEDGEMENTS

The authors would like to thank Wenhua Guo, Alanah Hallas, Manuel Brando, and Frank Steglich for fruitful discussions and Nicholas Botto for performing EMPA measurements. MS, CLH, and EM acknowledge support from the Gordon and Betty Moore Foundation EPiQS initiative through grant GBMF 4417. This publication is funded in part by a QuantEmX grant from ICAM and the Gordon and Betty Moore Foundation through Grant GBMF5305 to Macy L. Stavinoha. The work performed at University of California, Davis was supported by NSF-DMR-1709382. SGM was supported by the Director,

Office of Science, Office of Basic Energy Sciences, Division of Chemical Sciences, Geosciences, and Biosciences Heavy Element Chemistry Program of the U.S. Department of Energy (DOE) at LBNL under Contract No. DE-AC02-05CH11231. Eu M<sub>5,4</sub>-edge spectra described in this paper were measured at the Canadian Light Source, which is supported by the Canada Foundation for Innovation, Natural Sciences and Engineering Research Council

of Canada, the University of Saskatchewan, the Government of Saskatchewan, Western Economic Diversification Canada, the National Research Council Canada, and the Canadian Institutes of Health Research. TMM acknowledges support from the Johns Hopkins University Catalyst Award and a David and Lucile Packard Foundation Fellowship for Science and Engineering.

- 
- <sup>1</sup> M. Brian Maple, *J. Phys. Soc. Jpn.*, **74**, 222 (2005).
- <sup>2</sup> M. Nicklas, M. E. Macovei, J. Ferstl, C. Krellner, C. Geibel, and F. Steglich, *Phys. Status Solidi B*, **247**, 727 (2010).
- <sup>3</sup> T. Takabatake, F. Iga, T. Yoshino, Y. Echizen, K. Kato, K. Kobayashi, M. Higa, N. Shimizu, Y. Bando, G. Nakamoto, H. Fujii, K. Izawa, T. Suzuki, T. Fujita, M. Sera, M. Hiroi, K. Maezawa, S. Mock, H. v. Löhneysen, A. Brückl, K. Neumaier, and K. Andres, *J. Magn. Magn. Mater.*, **177-181**, 277 (1998).
- <sup>4</sup> T. N. Voloshok, N. V. Mushnikov, N. Tristan, R. Klingeler, B. Büchner, and A. N. Vasiliev, *Phys. Rev. B*, **76**, 172408 (2007).
- <sup>5</sup> Y. Ōnuki, A. Nakamura, F. Honda, D. Aoki, T. Tekeuchi, M. Nakashima, Y. Amako, H. Harima, K. Matsubayashi, Y. Uwatoko, S. Kayama, T. Kagayama, K. Shimizu, S. Esakki Muthu, D. Braithwaite, B. Salce, H. Shiba, T. Yara, Y. Ashitomi, H. Akamine, K. Tomori, M. Hedo and T. Nakama, *Philos. Mag.*, (2016).
- <sup>6</sup> Svilen Bobev, Eric D. Bauer, J.D. Thompson, and John L. Sarrao, *J. Magn. Magn. Mater.*, **277**, 236 (2004).
- <sup>7</sup> Ai Nakamura, Yuichi Hiranaka, Masato Hedo, Takao Nakama, Yasunao Miura, Hiroki Tsutsumi, Akinobu Mori, Kazuhiro Ishida, Katsuya Mitamura, Yusuke Hirose, Kiyohiro Sugiyama, Fuminori Honda, Rikio Settai, Tetsuya Takeuchi, Masayuki Hagiwara, Tatsuma D. Matsuda, Etsuji Yamamoto, Yoshinori Haga, Kazuyuki Matsubayashi, Yoshiya Uwatoko, Hisatomo Harima, and Yoshichika Ōnuki, *J. Phys. Soc. Jpn.*, **82**, 104703 (2013).
- <sup>8</sup> Ai Nakamura, Taro Uejo, Fuminori Honda, Tetsuya Takeuchi, Hisatomo Harima, Etsuji Yamamoto, Yoshinori Haga, Kazuyuki Matsubayashi, Yoshiya Uwatoko, Masato Hedo, Takao Nakama, and Yoshichika Ōnuki, *J. Phys. Soc. Jpn.*, **84**, 124711 (2015).
- <sup>9</sup> Beatriz Cordero, Verónica Gómez, Ana E. Platero-Prats, Marc Revés, Jorge Echeverría, Eduard Cremades, Flavia Barragán, and Santiago Alvarez, *Dalton Trans.*, 2832 (2008).
- <sup>10</sup> G. D. Loula, R. D. dos Reis, D. Haskel, F. Garcia, N. M. Souza-Neto, and F. C. G. Gandra, *Phys. Rev. B*, **85**, 245128 (2012).
- <sup>11</sup> Abishek K. Iyer, Lahari Balisetty, Sumanta Sarkar, and Sebastian C. Peter, *J. Alloys Compd.*, **582**, 305 (2014).
- <sup>12</sup> Paul H. Tobash and Svilen Bobev, *J. Alloys Compd.*, **418**, 58 (2006).
- <sup>13</sup> M. Stavinoha, *et al.*, in preparation.
- <sup>14</sup> Juan Rodríguez-Carvajal, *Physica B*, **192**, 55 (1993).
- <sup>15</sup> Stefan G. Minasian, Enrique R. Batista, Corwin H. Booth, David L. Clark, Jason M. Keith, Stosh A. Kozimor, Wayne W. Lukens, Richard L. Martin, David K. Shuh, S. Chantal E. Stieber, Tolek Tyliczszak, and Xiao-dong Wen, *J. Am. Chem. Soc.*, **139**, 18052 (2017).
- <sup>16</sup> Alison B. Altman, C. D. Pemmaraju, Selim Alayoglu, John Arnold, Eric D. Bauer, Corwin H. Booth, Zachary Fisk, Joseph I. Pacold, David Prendergast, David K. Shuh, Tolek Tyliczszak, Jian Wang, and Stefan G. Minasian, *Phys. Rev. B*, **97**, 045110 (2018).
- <sup>17</sup> Gordon J. Miller, Fan Li, and Hugo F. Franzenh, *J. Am. Chem. Soc.*, **115**, 3739 (1993).
- <sup>18</sup> G. Kaindl, G. Kalkowski, W. D. Brewer, B. Perscheid, and F. Holtzberg, *J. Appl. Phys.*, **55**, 1910 (1984).
- <sup>19</sup> B. T. Thole, G. van der Laan, J. C. Fuggle, G. A. Sawatzky, R. C. Karnatak, and J.-M. Esteve, *Phys. Rev. B*, **32**, 5107 (1985).
- <sup>20</sup> Michael E. Fisher, *Philos. Mag.*, **7**, 1731 (1962).
- <sup>21</sup> Neeraj Kumar, S. K. Dhar, A. Thamizhavel, P. Bonville, and P. Manfrinetti, *Phys. Rev. B*, **81**, 144414 (2010).
- <sup>22</sup> Z. Hossain, O. Trovarelli, C. Geibel, and F. Steglich, *J. Alloys Compd.*, **323-324**, 396 (2001).
- <sup>23</sup> A.R. Denton and N.W. Ashcroft, *Phys. Rev. A*, **43**, 3161 (1991).

## Appendix

Further details of the crystal structures in CIF format for  $\text{Eu}(\text{Ga}_{1-x}\text{Al}_x)_4$  with  $x = (0-1)$  may be obtained from FIZ Karlsruhe, 76344 Eggenstein-Leopoldshafen, Germany (fax: (+49)7247-808-666; e-mail: [crysdata\(at\)fiz-karlsruhe\(dot\)de](mailto:crysdata(at)fiz-karlsruhe(dot)de), on quoting the deposition numbers CSD-434440, -434441, -434442, -434443, -434444, and -434445.

### A. Summary of magnetic, transport, and crystallographic data

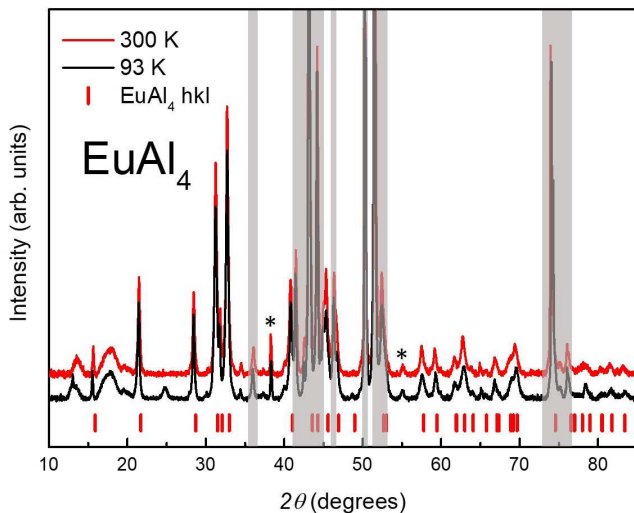


FIG. S1: Powder x-ray diffraction of  $\text{EuAl}_4$  performed at 300 K (red line) and 93 K (black line). This indicates that the tetragonal space group is preserved above and below the CDW-like transition, and the anomaly in resistivity is not caused by a structural phase transition. Gray bars indicate large background peaks from the metal sample holder and stars indicate the presence of small amounts of Al flux.

### B. Lattice parameters and band structure calculations for $\text{SrGa}_4$ , $\text{SrAl}_2\text{Ga}_2$ , and $\text{SrAl}_4$

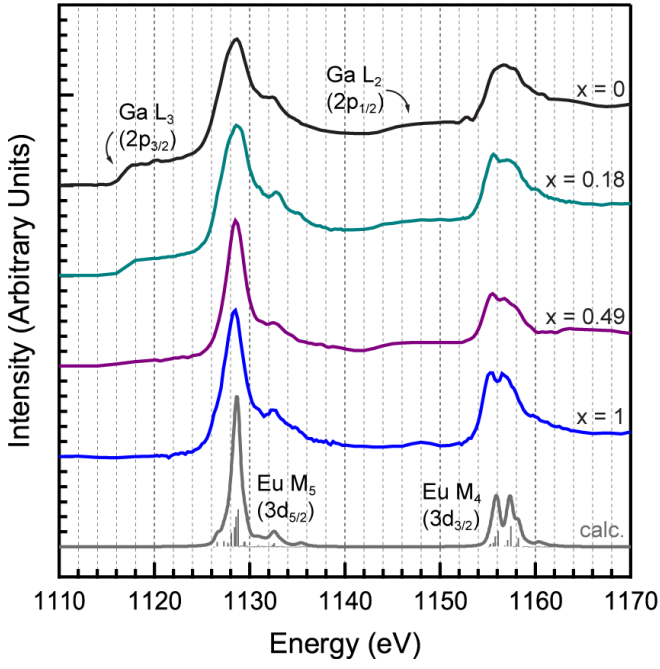


FIG. S2: Experimental Eu  $M_{5,4}$ -edge spectra of  $\text{Eu}(\text{Ga}_{1-x}\text{Al}_x)_4$  and configuration interaction calculation in the atomic limit for  $\text{Eu}^{2+}$ . Ga  $L_{3,2}$ -edge features emerge with decreased values of  $x$ .

TABLE S1: Crystallographic data for single crystals of  $\text{Eu}(\text{Ga}_{1-x}\text{Al}_x)_4$  (space group  $I4/mmm$ ). Values for  $x$  determined from EMPA.

parameter	$x = 0$	$x = 0.18$	$x = 0.33$	$x = 0.50$	$x = 0.68$	$x = 1$
$x$ from free variable refinement	0	0.15	0.31	0.47	0.68	1
$a$ ( $\text{\AA}$ )	4.3904(7)	4.381(3)	4.3551(9)	4.3301(7)	4.3429(13)	4.4113(9)
$c$ ( $\text{\AA}$ )	10.6720(18)	10.757(7)	10.833(2)	10.9253(17)	11.018(3)	11.204(3)
$V$ ( $\text{\AA}^3$ )	205.71(7)	206.5(3)	205.47(9)	204.85(7)	207.80(14)	218.02(11)
absorption coefficient ( $\text{mm}^{-1}$ )	40.640	36.87	32.93	29.14	23.57	14.968
measured reflections	1656	969	1734	1725	1769	1722
independent reflections	137	92	138	139	139	140
$R_{int}$	0.036	0.031	0.022	0.017	0.047	0.048
goodness-of-fit on $F^2$	1.23	1.20	1.28	1.20	1.12	1.529
$R_1(F)$ for $F_o^2 > 2\sigma(F_o^2)^a$	0.014	0.024	0.012	0.009	0.015	0.018
$wR_2(F_o^2)^b$	0.037	0.057	0.029	0.021	0.025	0.038
extinction coefficient	0.0127(11)	0.0022(13)	0.0103(9)	0.0019(5)	0.0019(8)	0.0057(15)
temperature (K)	90	90	90	90	90	188

$$^a R_1 = \sum || F_o | - | F_c || / \sum | F_o | \quad ^b wR_2 = [\sum [w(F_o^2 - F_c^2)^2] / \sum [w(F_o^2)^2]]^{1/2}$$

TABLE S2: Summary of magnetic and transport properties in  $\text{Eu}(\text{Ga}_{1-x}\text{Al}_x)_4$ 

$x$	$T_N$ (K) <sup>a</sup> $T_2$ (K) <sup>a</sup> $T_3$ (K) <sup>a</sup>	$T_N$ (K) <sup>b</sup> $T_2$ (K) <sup>b</sup> $T_3$ (K) <sup>b</sup>	$T_N$ (K) <sup>c</sup> $T_2$ (K) <sup>c</sup> $T_3$ (K) <sup>c</sup>	$p_{eff}$	$M_0$ (emu/mol <sub>Eu</sub> )	$\theta_W$ (K)	$H_{c1}$ (T) $H_{c2}$ (T) $H\parallel ab$	$H_{c1}$ (T) $H_{c2}$ (T) $H\parallel c$	RRR	$T^*$ (K)
0	15.9 13.3	15.9	16.2	8.13	0.0015	6.64	>7 0.6	>7 1	54	
0.18	12.4 8.4	12.4 8.9	12.7	7.91	0	11.16	4.0	4.3	3.6	
0.33	14.9 12.9	14.9 13.4	15.4 13.6	8.15	0	12.26	2.5	3.3 2.4 1.0	1.4	
0.50	17.4 15.4 10.4	18.4 14.9 10.9	19.0 15.6 10.9	7.96	0	22.59	1.5 0.6 0.3	2.4 1.6 1.0	6.1	51
0.68	18.4 15.9	18.4 15.9	19.1 16.4	8.23	0	17.82	1.4 0.9 0.2	2.1 1.5 0.5	4.9	
1	14.9 12.4 10.4	14.4 11.9 10.4	15.2 13.3 12.3	7.98	0	15.02	1.6 1.4	1.8 1.3 1.0	70	141

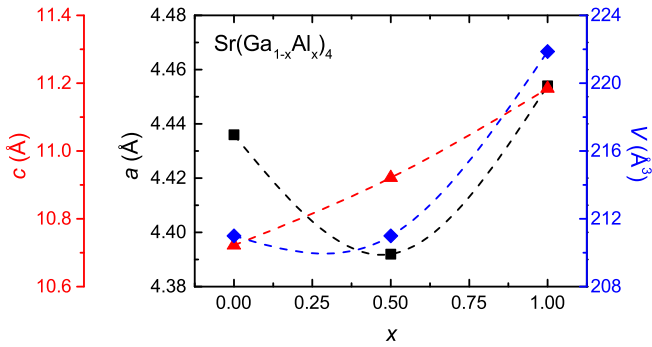
<sup>a</sup>from  $d(MT)/dT$  with  $H\parallel ab$ <sup>b</sup>from  $d(MT)/dT$  with  $H\parallel c$ <sup>c</sup>from  $C_p(T)$ 

FIG. S3: Lattice parameters from powder x-ray diffraction of  $\text{SrGa}_4$ ,  $\text{SrAl}_2\text{Ga}_2$ , and  $\text{SrAl}_4$  single crystals. Trends seen here are consistent with trends observed in the Eu analogues, indicating that the non-linear change in  $a$  is associated with the Ga–Al sublattice.

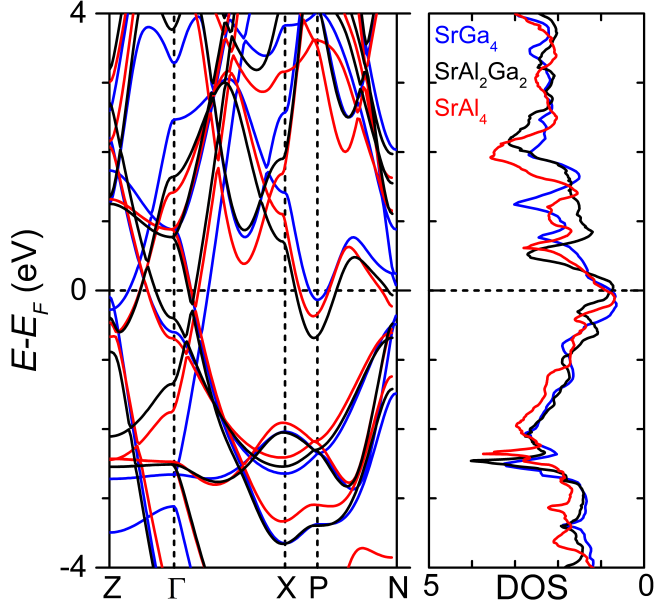


FIG. S4: Band structure calculations for  $\text{SrGa}_4$ ,  $\text{SrAl}_2\text{Ga}_2$ , and  $\text{SrAl}_4$ .  $\text{Sr}^{2+}$  is used as a substitute for  $\text{Eu}^{2+}$  to avoid complications arising from unpaired  $4f$  electrons.

TABLE S3: Analysis of the electron distribution extracted from the integrated density of states up to  $E_F$  provides insight into the polarization of the Ga–Al bonds. In contrast to both end members, in  $\text{SrAl}_2\text{Ga}_2$  there is increased charge transfer to the  $M(2)$  site. This charge transfer only manifests when  $M(1) = \text{Al}$  and  $M(2) = \text{Ga}$ , implying an enhanced polarization in the  $M(1)–M(2)$  covalent bonds in  $\text{SrAl}_2\text{Ga}_2$ .

compound	$e^-/M(1)$	$e^-/M(2)$
$\text{SrGa}_4$	5.70	4.40
$\text{SrAl}_4$	5.63	4.40
$\text{SrAl}_2\text{Ga}_2$	5.50	4.70
$\text{SrGa}_4$	5.56	4.40
(with $\text{SrAl}_2\text{Ga}_2$ structure parameters)		
$\text{SrAl}_4$	5.75	4.30
(with $\text{SrAl}_2\text{Ga}_2$ structure parameters)		